

**METAL OXIDE BASED SEMICONDUCTORS FOR
SUSTAINABILITY AND SENSING BASED
APPLICATIONS**

Siddharth Rana



DEPARTMENT OF PHYSICS

INDIAN INSTITUTE OF TECHNOLOGY DELHI

July 2025

©Indian Institute of Technology Delhi (IITD), New Delhi, 2025

**METAL OXIDE BASED SEMICONDUCTORS FOR
SUSTAINABILITY AND SENSING BASED
APPLICATIONS**

by

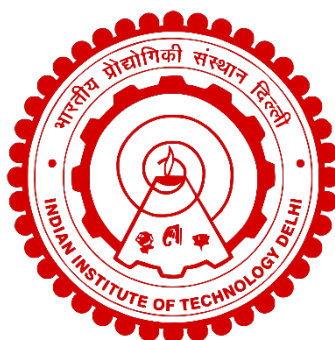
Siddharth Rana

Department of Physics

Submitted

in fulfilment of requirements of degree of Doctor of Philosophy

to the



INDIAN INSTITUTE OF TECHNOLOGY DELHI

July 2025

Dedication

I dedicate this dissertation to my parents, **Mr. Dushyant Rana** and **Mrs. Seema Rana**, whose unwavering support, blessings, and encouragement have been a constant source of strength and inspiration in my journey.

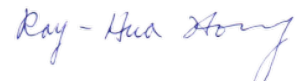
CERTIFICATE

We certify that the thesis titled “**METAL OXIDE-BASED SEMICONDUCTORS FOR SUSTAINABILITY AND SENSING APPLICATIONS**”, submitted by Mr. Siddharth Rana, is a genuine and original research work conducted under our supervision. In our assessment, the thesis meets the necessary standards and is worthy of consideration for the degree of Doctor of Philosophy. The findings presented in this thesis have not been submitted, either in whole or in part, to any other university or institute for the award of a degree or diploma.



Prof. J.P. Singh

Department of Physics
Indian Institute of Technology Delhi
New Delhi-110016, India



Prof. Ray Hua Horng

Institute of electronics
National Yang Ming Chiao Tung University
Hsinchu, Taiwan

Date: 8th July 2025

ACKNOWLEDGEMENTS

The journey of this doctoral thesis would not have been possible without the unwavering support and contributions of many individuals who have created a stimulating and productive environment for my research. I am deeply grateful to everyone who has played a role in shaping my academic path and enabling me to successfully complete this work.

*First and foremost, I extend my sincere gratitude to my thesis supervisors, **Prof. J.P. Singh** and **Prof. Ray-Hua Horng**, for their invaluable guidance, encouragement, and expertise. Their profound knowledge, patience, and unwavering commitment have been instrumental in shaping the direction of my research. I am truly fortunate to have learned from their wisdom and experience.*

*I am also deeply appreciative of my SRC members **Prof. Rajendra Singh Dhaka**, **Prof. Saswata Bhattacharya**, and **Prof. Sreedevi Upadhyayula** for their insightful suggestions, continuous support, and ever-helpful approach throughout my doctoral journey.*

I am grateful to the MFIRP scheme at IIT Delhi for providing me with the opportunity to be part of the joint degree program, an experience that has greatly enriched my academic and research perspective.

*My heartfelt thanks go to my colleagues at **GLAD and ASTDL Lab**, whose collaboration and camaraderie have made this journey both intellectually stimulating and enjoyable. I extend my appreciation to **Dr. Yogita Maithani**, **Dr. Jyoti Yadav**, **Dr. Sarjana Yadav**, **Dr. Jamal Ahmed Khan**, **Dr. Arvind**, **Sneha Senapati**, **Shivam Singh**, **Vidhya**, **Lakshay**, **Debottam**, **Deepali**,*

Vandana, and **Priyanka** for fostering a supportive and enriching research environment. A special note of thanks to **Jyoti (Anshul)** for her invaluable assistance, both technically and beyond, throughout my research.

I would also like to express my gratitude to **Dr. F.G. Tarntair, Chih-Yang Huang, Yu-Hsuan Hsu, Clay, Will** and **Soumitra Shubhankar**, as well as the entire **ASTDL lab team**, for their collaboration, valuable suggestions, and their meticulous efforts in improving the quality of my research. Their willingness to share knowledge and engage in thoughtful discussions has been immensely beneficial.

A true friend is a light in both sunshine and storms, standing by you through every season of life. I am incredibly fortunate to have had the support of my dear friends **Mr. Sandeep Kumar, Ms. Sneha Senapati, Mr. Kamlesh Bhatt, Mr. Uzair Alam, Mr. Harish Khan, Mr. Gopal Singh**, and **Ms. Pratibha**, who stood by my side during both the challenges and triumphs of my research journey. Their friendship and encouragement have been a source of strength and motivation.

A special thanks to my family for their unconditional love, patience, and belief in me. Their unwavering support has been the foundation that has allowed me to pursue my academic aspirations. I am especially grateful to my siblings, **Parth Rana** and **Alice Chauhan**, whose constant encouragement and guidance have been invaluable in both my personal and academic life.

I gratefully acknowledge the **Council of Scientific and Industrial Research (CSIR)** for funding my research through the Research Fellowship.

Above all, I am profoundly grateful to Almighty God for granting me the wisdom, health, and perseverance to navigate this journey

.

Siddharth Rana

ABSTRACT

Metal oxide semiconductors are known for their exceptional chemical and thermal stability, making them ideal for a wide range of applications, including optoelectronics, energy harvesting, and catalysis. Their inherent structural robustness, resistance to environmental degradation, and tunable electronic properties enable their integration into high-performance electronic and photonic devices.

This thesis focuses on the growth and application of metal oxides for X-ray and ultraviolet (UV) detection, with additional investigations into their potential use in power devices and photoelectrochemical water splitting. The interaction of incident light with semiconductor materials leads to the generation of electron-hole pairs, a fundamental process that underpins both photodetection and energy conversion applications.

The first phase of this research explores the growth and characterization of ZnGa_2O_4 epilayers synthesized via metal-organic chemical vapor deposition (MOCVD) for direct hard X-ray detection. The results demonstrate that ZnGa_2O_4 exhibits a remarkably high sensitivity of $2.87 \times 10^9 \mu\text{C Gy}_{\text{air}}^{-1}\text{cm}^{-2}$ to X-rays, attributed to its high density and strong absorption capabilities. Furthermore, an in-depth analysis of the dose-dependent response reveals that ZnGa_2O_4 enables efficient low-dose X-ray detection, significantly outperforming Ga_2O_3 , which failed to achieve the same level of sensitivity. Notably, ZnGa_2O_4 exhibited an enhancement of nearly four orders of

magnitude compared to Ga_2O_3 , underscoring its potential as a superior material for X-ray sensing applications.

In the second phase, ZnGa_2O_4 thin films were utilized to fabricate thin-film transistors (TFTs) to further investigate their optoelectronic properties. A systematic study on the influence of device geometry, specifically varying the source-to-drain distance from 20 to 40 μm , revealed that shorter channel lengths facilitated faster charge carrier collection, enhancing the material's photodetection capabilities. Conversely, longer channel lengths exhibited a breakdown voltage of approximately 656 V, making them suitable for high-power applications. Additionally, enhancement-mode and depletion-mode TFTs were successfully fabricated by controlling the epilayer thickness from 85 nm to 135 nm, with thinner films exhibiting E-mode characteristics due to complete depletion across the channel. The Inductively coupled plasma etched sample showed responsivity and rejection ratio at 240 nm was 128.5 A/W and 10^5 at a gate voltage of -10 V. To optimize the performance of ZnGa_2O_4 -based phototransistors, the role of defect engineering was explored through neutral ion beam etching. This process effectively minimized sidewall leakage and improved response times, leading to enhanced device stability and performance. The use of neutral ion beam technology showed an improvement in the phototransistor responsivity up to 296.8 A/W (at 240 nm) @ $5.6\mu\text{W cm}^{-2}$. The combination of high sensitivity, low defect density, and superior phototransistor performance highlights ZnGa_2O_4 as a promising candidate for UV-C photodetection.

The optical and electrical properties of metal oxides play a crucial role in their functional applications. In the following work, the properties of ZnGa₂O₄ were systematically modified using swift heavy ion irradiation. The ZnGa₂O₄ film was exposed to 120 MeV gold ions with varying fluence from 10¹² to 10¹³ ions cm⁻², and the resulting structural and electronic changes were analyzed. The findings confirmed the radiation resistance of ZnGa₂O₄, demonstrating its stability under high-energy ion exposure. A notable reduction in the bandgap was observed, decreasing from 4.91 eV to 4.21 eV, indicating enhanced optical tunability. Additionally, the wettability of the film transitioned to a hydrophilic nature, aligning with XPS results that suggested surface chemical modifications. Furthermore, ion irradiation significantly influenced the electrical properties of ZnGa₂O₄. The sheet resistance exhibited a two-order reduction, decreasing from 290 MΩ/□ to just 1.9 MΩ/□, which is a crucial improvement for high-performance power devices that require low resistivity. These tunable characteristics establish ZnGa₂O₄ as a contender for optoelectronic and power applications, where controlled electrical and optical properties are essential.

In the final work, photoelectrochemical water splitting was investigated using CuO/Cu₂O/Cu-based electrodes to explore their potential for sustainable hydrogen production. Copper oxide nanowires were synthesized under different ambient conditions, including air, oxygen, and argon, leading to variations in their morphology and optical absorption properties. The composition of CuO and Cu₂O varied across the samples, influencing their surface wettability, with contact angles ranging from 32.6° to 101.6°. Among

the synthesized electrodes, the one prepared in an oxygen-rich environment exhibited the highest photocurrent density of 1.8 mA cm^{-2} at -0.5 V , indicating enhanced charge separation and improved photoelectrochemical performance. These findings demonstrate the critical role of ambient conditions in tailoring the properties of copper oxide nanostructures and highlight their potential for efficient hydrogen generation through water splitting. This study reinforces the viability of metal oxides as key materials for sustainable energy applications.

सारांश

यह शोधप्रबंध धातु ऑक्साइड अर्धचालकों की उत्कृष्ट रासायनिक और तापीय स्थिरता को रेखांकित करता है, जो इन्हें ऑप्टोइलेक्ट्रॉनिक्स, ऊर्जा संचयन और उत्प्रेरण (कैटलिसिस) सहित विभिन्न अनुप्रयोगों के लिए उपयुक्त बनाता है। इनकी संरचनात्मक मजबूती, पर्यावरणीय गिरावट के प्रति प्रतिरोधक क्षमता और इलेक्ट्रॉनिक गुणों की अनुकूलनशीलता इन्हें उच्च प्रदर्शन वाले इलेक्ट्रॉनिक और फोटोनिक उपकरणों में उपयोग के लिए सक्षम बनाती है।

यह शोध मुख्य रूप से एक्स-रे और पराबैंगनी (UV) विकिरण की पहचान के लिए धातु ऑक्साइडों की वृद्धि और अनुप्रयोग पर केंद्रित है, साथ ही पावर डिवाइसों और फोटोइलेक्ट्रोकेमिकल जल अपघटन में उनके संभावित उपयोग का भी अध्ययन किया गया है। अर्धचालक सामग्री पर प्रकाश पड़ने से इलेक्ट्रॉन-होल युग्म उत्पन्न होते हैं, जो फोटोडिटेक्शन और ऊर्जा रूपांतरण जैसे अनुप्रयोगों की आधारभूत प्रक्रिया है।

शोध के पहले चरण में, हार्ड एक्स-रे पहचान के लिए मेटल-ऑर्गेनिक केमिकल वेपर डिपॉजिशन (MOCVD) तकनीक द्वारा $ZnGa_2O_4$ एपिलेयर्स की वृद्धि और वर्णन किया गया। $ZnGa_2O_4$ ने $2.87 \times 10^9 \mu C Gy_{air}^{-1} cm^{-2}$ की उच्च संवेदनशीलता प्रदर्शित की, जो इसकी उच्च घनता और मजबूत अवशोषण क्षमताओं के कारण है। डोज-निर्भर प्रतिक्रिया विश्लेषण से ज्ञात हुआ कि $ZnGa_2O_4$ कम डोज पर भी कुशलतापूर्वक एक्स-रे पहचान करने में सक्षम है, जबकि Ga_2O_3 इतनी संवेदनशीलता प्रदर्शित नहीं कर पाया। $ZnGa_2O_4$ ने Ga_2O_3 की तुलना में लगभग चार गुणात्मक श्रेणियों तक बेहतर प्रदर्शन किया, जो इसे एक्स-रे डिटेक्शन के लिए एक उत्कृष्ट सामग्री सिद्ध करता है।

दूसरे चरण में, $ZnGa_2O_4$ की ऑप्टोइलेक्ट्रॉनिक विशेषताओं को जांचने के लिए इसका उपयोग पतली फिल्म ट्रांजिस्टर (TFTs) निर्माण में किया गया। डिवाइस ज्यामिति, विशेष रूप से स्रोत और ड्रेन के बीच

दूरी (20 से 40 माइक्रॉन) को बदलकर किए गए अध्ययन से पता चला कि छोटे चैनल लंबाई से चार्ज कैरियर्स का तेजी से संग्रहण संभव हुआ, जिससे फोटोडिटेक्शन क्षमता में सुधार हुआ। वहीं, बड़े चैनल की लंबाई पर लगभग 656 V का ब्रेकडाउन वोल्टेज देखा गया, जो उच्च शक्ति अनुप्रयोगों के लिए उपयुक्त है। एपिलयर मोटाई (85 nm से 135 nm) को नियंत्रित कर E-mode और D-mode TFTs बनाए गए, जहाँ पतली फिल्मों ने E-mode व्यवहार दिखाया। इंडक्टिवली कपल्ड प्लाज़्मा द्वारा एच की गई फिल्म ने 240 nm पर -10 V गेट वोल्टेज पर 128.5 A/W रिस्पॉन्सिविटी और 105 का रीजेक्शन रेशियो प्रदर्शित किया। $ZnGa_2O_4$ -आधारित फोटोट्रांजिस्टर की कार्यक्षमता को अनुकूलित करने के लिए न्यूट्रल आयन बीम एचिंग तकनीक का उपयोग किया गया, जिससे साइडवॉल लीकेज कम हुआ और रिस्पॉन्स टाइम बेहतर हुआ। इसके परिणामस्वरूप 240 nm पर 296.8 A/W की रिस्पॉन्सिविटी ($5.6 \mu W cm^{-2}$ पर) प्राप्त हुई। उच्च संवेदनशीलता, कम डिफेक्ट डेंसिटी और श्रेष्ठ प्रदर्शन $ZnGa_2O_4$ को UV-C फोटोडिटेक्शन के लिए एक संभावनाशील सामग्री बनाते हैं।

धातु ऑक्साइड की ऑप्टिकल और इलेक्ट्रिकल विशेषताएँ उनके कार्यात्मक अनुप्रयोगों में महत्वपूर्ण भूमिका निभाती हैं। आगे के अध्ययन में, $ZnGa_2O_4$ की विशेषताओं को स्विफ्ट हेवी आयन विकिरण द्वारा व्यवस्थित रूप से संशोधित किया गया। $ZnGa_2O_4$ फिल्म को 120 MeV स्वर्ण आयनों से 10^{12} से 10^{13} आयन cm^{-2} की फ्लुएंस पर विकिरणित किया गया और इसके संरचनात्मक एवं इलेक्ट्रॉनिक परिवर्तन का विश्लेषण किया गया। परिणामों ने $ZnGa_2O_4$ की विकिरण प्रतिरोध क्षमता को प्रमाणित किया, जो इसे उच्च ऊर्जा विकिरण के तहत स्थिर सिद्ध करता है। बैंडगैप में उल्लेखनीय कमी देखी गई, जो 4.91 eV से घटकर 4.21 eV हो गया, जिससे इसके ऑप्टिकल गुणों में ट्यूनिंग की संभावना उजागर हुई। इसके अलावा, फिल्म की वेतेबिलिटी हाइड्रोफिलिक प्रकृति में बदल गई, जो XPS परिणामों से मेल खाती है जो सतही रासायनिक परिवर्तन का संकेत देती है। विद्युत गुणों में भी बड़ा परिवर्तन देखा गया; शीट रेजिस्टेंस में दो आदेशों की कमी आई— $290 M\Omega/\square$ से घटकर केवल $1.9 M\Omega/\square$ —जो उच्च प्रदर्शन वाले पावर

डिवाइसों के लिए अत्यंत उपयोगी है। ये अनुकूलनीय गुण $ZnGa_2O_4$ को ऑटोइलेक्ट्रॉनिक और पावर अनुप्रयोगों के लिए एक प्रबल दावेदार बनाते हैं।

अंतिम अध्ययन में, $CuO/Cu_2O/Cu$ आधारित इलेक्ट्रोड्स का उपयोग कर फोटोइलेक्ट्रोकेमिकल जल अपघटन द्वारा स्थायी हाइड्रोजन उत्पादन की संभावना का मूल्यांकन किया गया। तांबा ऑक्साइड नैनोवायर विभिन्न वातारण स्थितियों—वायु, ऑक्सीजन और आर्गन—में संश्लेषित किए गए, जिससे उनकी संरचना और ऑप्टिकल अवशोषण विशेषताओं में भिन्नता देखी गई। CuO और Cu_2O की संरचना में अंतर के कारण संपर्क कोण 32.6° से 101.6° तक अलग-अलग थे। ऑक्सीजन-समृद्ध वातावरण में तैयार किए गए इलेक्ट्रोड ने -0.5 V पर 1.8 mA cm^{-2} की सर्वाधिक फोटोक्रेन्ट डेंसिटी प्रदर्शित की, जो बेहतर चार्ज पृथक्करण और बेहतर फोटोइलेक्ट्रोकेमिकल प्रदर्शन को दर्शाता है। यह अध्ययन दर्शाता है कि तांबा ऑक्साइड नैनोस्ट्रक्चर्स के गुणों को नियंत्रित करने में परिवेशीय परिस्थितियाँ कितनी महत्वपूर्ण हैं, और यह इन्हें जल अपघटन द्वारा कुशल हाइड्रोजन उत्पादन के लिए उपयुक्त बनाता है। यह शोध धातु ऑक्साइडों को सतत ऊर्जा अनुप्रयोगों के लिए प्रमुख सामग्री के रूप में स्थापित करता है।

TABLE OF CONTENTS

CERTIFICATE	i
ACKNOWLEDGEMENTS	ii
ABSTRACT	v
सारांश	ix
TABLE OF CONTENTS	xii
LIST OF FIGURES	xvi
LIST OF TABLES	xxii
ABBREVIATIONS	xxiii
Chapter 1: Introduction	1-25
1.1 Metal oxides: Versatile Materials for Next-Gen Sensing and Energy Applications	2
1.2. Transitioning from Silicon electronics: Ultrawide bandgap semiconductors.....	5
1.3 Key Concepts:	6
1.3.1 Basics of photodetection	6
1.3.2 Swift heavy ion irradiation.....	7
1.3.3 Photoelectrochemical water splitting.....	8
1.4 Materials of Interest:	10
1.4.1 Zinc Gallium Oxide:.....	10
1.4.2 Cuprous Oxide and Cupric Oxide:	11
1.5 Device Structures and Mechanisms:.....	14
1.5.1 Photodetectors	14
1.5.2 Heterojunctions for PEC water splitting	16
1.6 Performance parameters:	18
1.6.1 Performance parameters of PD	18
1.6.2 Performance parameters for power devices	20
1.6.3 Performance parameters for water splitting.....	21
1.7 Objectives:	22
1.8 Thesis Overview:	22
Chapter 2: Experimental techniques and characterization	26-48
2.1 Growth Techniques	27

2.1.1 Metalorganic chemical Vapor deposition	27
2.1.2 Atomic layer deposition	28
2.1.3 E-Beam deposition	29
2.1.4 Thermal Oxidation in Chemical vapor deposition chamber.....	30
2.2 Characterization Techniques:	32
2.2.1 X-ray diffraction measurements.....	32
2.2.2 Electron microscopy	34
2.2.2.1 Field emission scanning electron microscope	34
2.2.2.2 Electron probe Microanalyzer	35
2.2.3 Atomic force Microscopy	36
2.2.4 UV-Visible spectroscopy	38
2.2.4 X-ray photoelectron spectroscopy	40
2.2.5 Contact angle measurements	41
2.3 Fabrication Techniques:	42
2.3.1 Photolithography:	43
2.3.2 Etching	44
2.4 Electrical characterization	45
2.4.1 Semiconductor parameter analyzer:.....	45
2.2 Photoelectrochemical Measurements	46
Chapter 3: Direct hard X-ray detection using Metal-Semiconductor-Metal	
ZnGa₂O₄-based detector.....	49-73
3.1 Introduction	50
3.2 Experiment	52
3.2.1 Growth of ZnGa ₂ O ₄ and Ga ₂ O ₃ epilayers	52
3.2.2 Fabrication of the DXPD	53
3.2.3 Structural and photoresponse characterization	53
3.2.4 DFT Calculations.....	53
3.3 Results and discussion:	54
3.3.1 Structural characterization and current-voltage properties	54
3.3.2 Performance of DXPD with hard X-rays exposure	57
3.3.3 Response Mechanism of Wide Bandgap DXPDs	62
3.3.4 DFT calculations	68
3.4 Conclusions	73

Chapter 4: Study of source-to-drain distance variation in ZnGa₂O₄ thin-film transistors for UV-C detection and power applications.....74-107

4.1 Introduction 75

4.2 Experiment: 80

 4.2.1 Growth of ZnGa₂O₄ epilayer 80

 4.2.2 Fabrication of ZnGa₂O₄ TFT 80

 4.2.3 Characterization..... 83

4.3 Results and Discussions 84

 4.3.1 Morphological and structural analysis 84

 4.3.2 Optical properties and Chemical composition: 85

 4.3.3 Device Mapping and TLM Measurements: 88

 4.3.4 Transfer and output characteristics of neutral ion beam etched TFT 90

 4.3.5 Breakdown Characteristics..... 94

 4.3.6 Photoresponse Measurements of ICP etched PT: 96

 4.3.7 Neutral Ion- beam etched Phototransistor:..... 105

4.4 Conclusions: 106

Chapter 5: Effect of swift heavy gold ion irradiation on the optical and electrical properties of ZnGa₂O₄ thin-film for optoelectronic applications108-129

5.1 Introduction 109

5.2 Experimental: 112

 5.2.1 Growth of ZnGa₂O₄ film..... 112

 5.2.2 Fabrication of Transmission line measurement contacts on ZnGa₂O₄ film 112

 5.2.3 Characterization..... 113

5.3 Results and discussion 114

 5.3.1 SRIM simulation..... 114

 5.3.2 Structural and morphological characterization 115

 5.3.3 Chemical composition and optical properties 118

 5.3.4 Wetting properties 122

 5.3.5 Electrical characterization 124

5.4 Conclusions 129

Chapter 6: Photoelectrochemical water splitting based on CuO/Cu₂O/Cu based electrodes.....130-154

6.1 Introduction.....	131
6.2 Experimental:	134
6.2.1 Growth of copper oxide nanowires	134
6.2.2 Characterization.....	135
6.3 Results and discussion:	136
6.3.1 Structural and morphological characterization	136
6.3.2 Optical and chemical characterization	141
6.3.3 Wetting Properties	146
6.3.4 Photoelectrochemical Measurements	148
6.4 Conclusion.....	154
Chapter 7: Conclusion and Future prospective of Work.....	155-159
7.1 Summary and Conclusions:	156
7.2 Future Scope:	158
References	160
Publications	177
Biodata	180

LIST OF FIGURES

Figure 1. 1: Applications of Deep UV and X-ray photodetectors.	3
Figure 1. 2: The four generations of the semiconductor technology.....	5
Figure 1. 3: Schematic illustration of the photodetection ²⁶	7
Figure 1. 4: Illustration of the water splitting on a semiconductor.	9
Figure 1. 5: Crystal structure of ZnGa ₂ O ₄ simulated by vesta software.	10
Figure 1. 6: Crystal structure of the CuO and Cu ₂ O[32].....	12
Figure 1. 7: Schematic of different structures: (A) photoconductive MSM, (B) photovoltaic p-n junction, (C) avalanche p-n junction, and (D) phototransistor.	14
Figure 1. 8: Schematic energy band structure of ZnGa ₂ O ₄ PDs: (A) photoconductive MSM, (B) photovoltaic p-n junction, (C) avalanche p-n junction, and (D) phototransistor.	15
Figure 1. 9: Illustration of the types of heterojunctions (a) straddling-gap, (b) staggered-gap, and (c) broken gap.	17
Figure 2.1: Schematic of metalorganic chemical vapor deposition chamber	28
Figure 2.2: (a) Schematic of e-beam evaporation, and (b) image of actual setup.	30
Figure 2.3: Schematic of the chemical vapor deposition setup.	31
Figure 2.4: (a) Diffraction of X-rays from parallel planes, and (b) schematic of X-ray diffractometer.	32
Figure 2.5: Schematic of the FESEM setup, and (b) image of the FESEM TESCAN.....	35
Figure 2.6: Image of the electron probe microanalyzer (EPMA-1720 HT).....	36
Figure 2.7: Schematic of the atomic force microscopy.....	37
Figure 2. 8: Schematic diagram of UV-Visible spectroscopy.	39
Figure 2. 9: (a) Ejection of core electron by the incident X-rays, and (b) image of the XPS instrument (AXIS Supra).	40
Figure 2.10: (a) Image of the Kruss DSA25E drop shape analyzer, and (b) schematic showing two regime of wettability.....	42

Figure 2.11: Image of the (a) Double side mask aligner, (b) Wet bench, (c) optical microscope, (d) Optical profilometer, and (e) Spin coater used for PR coating.....	43
Figure 2.12: (a) Image of the ICP Chamber, and (b) Neutral ion beam process.	45
Figure 2.13: (A) Photodetector measurement system (B) Breakdown voltage measurement system, (c) 4155B semiconductor parameter analyzer, and (d) Keysight B1505 A system.....	46
Figure 2.14: (a) Schematic of the three-electrode system, and (b) image of the PEC setup.....	47
Figure 3. 1: The plots of high-resolution XRD. (a) High-resolution XRD patterns of the ZnGa ₂ O ₄ and β-Ga ₂ O ₃ epilayers. (b) Rocking curve of the (111) plane and (c) the phi (Φ) scan curve of the ZnGa ₂ O ₄ epilayer. (d) Rocking curve and (e) the phi (Φ) scan curve of the Ga ₂ O ₃ epilayer.....	55
Figure 3. 2: Current-voltage (I-V) for the fabricated MSM (a) ZnGa ₂ O ₄ DXPD, and (b) Ga ₂ O ₃ DXPD from -20 V to 20 V in a dark cabinet.....	57
Figure 3. 3: The setup for measuring photodetector characteristics using the ZnGa ₂ O ₄ epilayer.	58
Figure 3. 4: The photoresponse of a photodetector made for ZnGa ₂ O ₄ and β-Ga ₂ O ₃ when exposed to hard X-rays at different irradiation-dose levels: (a)-(c) for ZnGa ₂ O ₄ and (d)-(f) for β-Ga ₂ O ₃	59
Figure 3. 5: Interaction of X-rays with the (a) Crystal structure of ZnGa ₂ O ₄ and β-Ga ₂ O ₃ visualized by Vesta showing a higher absorption in the case of ZnGa ₂ O ₄ (b) atomic structure.	64
Figure 3. 6: (a) Photocurrent versus dose rate for the ZnGa ₂ O ₄ DXPDs (b) Sensitivity as a function of the applied biasing voltage for the ZnGa ₂ O ₄ and Ga ₂ O ₃ DXPDs.....	66
Figure 3. 7: (a) β-Ga ₂ O ₃ (-201) and (b) ZnGa ₂ O ₄ (111) excited by the absorption of X-rays (blue curves enter thin films vertically) and excited-state scattering (red curves leave thin films), and Band structure and partial density of states of ((c) Ga ₁₆ O ₂₄ and Ga ₁₆ O ₂₃ (d) Zn ₈ Ga ₁₆ O ₃₂ and Zn ₈ Ga ₁₆ O ₃₁ at the GGA+U level.	71
Figure 4. 1: Fabrication flow of the ZnGa ₂ O ₄ -based TFT.	81

Figure 4. 2: (a) Fabricated Phototransistor on the ZnGa ₂ O ₄ epilayer grown on c-plane sapphire substrate and (b) alignment keys of the mask.	81
Figure 4. 3: (a) Schematic of fabricated TFT and OM images of TFTs (b) showing gate length, and devices with (c) 40 μm L _{ds} and 30 μm L _{gd} , (d) 30 μm L _{ds} and 20 μm L _{gd} , and (e) 20 μm L _{ds} and 10 μm L _{gd}	82
Figure 4. 4: (a) 2 theta scan, (b) Phi scan and AFM image of (b) topography, and (c) 3D view of the grown ZnGa ₂ O ₄ epilayer.	84
Figure 4. 5: (a) Absorbance spectra, (b) Tauc plot, and spectroscopic ellipsometry measurements of (c) psi and delta, and (d) n and k of ZnGa ₂ O ₄ epilayer.....	86
Figure 4. 6: XPS (a) survey spectrum, (b) Zn 2p spectrum, (c) Ga 2p spectra, and (c) O 1s spectrum of grown ZnGa ₂ O ₄ epilayer.	87
Figure 4. 7: Microscope image of PT and EPMA mappings for Zn, Ga, O, Ti, Al, and Ni.....	89
Figure 4. 8: TLM characteristics (a) Current versus voltage at different distances and (b)Resistance versus distance.....	90
Figure 4. 9: The I _D -V _{GS} characteristics of the ZnGa ₂ O ₄ -based TFT with L _{ds} of (a) 20 μm, (b)30 μm, (c) 40 μm, and (d) Extraction of the V _{TH} from I _D -V _{GS} at V _{DS} = 10 V for different source to drain lengths.	92
Figure 4. 10: The I _D -V _{DS} characteristics of the ZnGa ₂ O ₄ -based TFT with L _{ds} of (a) 20 μm, (b)30 μm, (c) 40 μm, and (d) DIBL and Ron plot as a function of source to drain length.	93
Figure 4. 11: Breakdown characteristics of the ZnGa ₂ O ₄ -based TFT with L _{ds} of (a) 20 μm, (b)30 μm, (c) 40 μm, and (d) breakdown voltage as a function of source to drain length.	94
Figure 4. 12: (a) Transfer characteristics (I _D -V _G), (b) I _D -V _G with different incident light wavelengths, (c) variation of threshold voltage with the incident light wavelengths, and (d) output characteristics (I _D -V _D).	98
Figure 4. 13: (a) Responsivity as a function of wavelength, (b) Rise time, (c) fall time response, and (d) Power density versus photocurrent and responsivity plot of the fabricated PT at V _{GS} = -10 V and drain voltage 2 V.	100
Figure 4. 14: Photo-to-Dark Current Ratio (PDCR) of the fabricated PT...	102

Figure 4. 15: ZnGa ₂ O ₄ -based E-mode phototransistor (a) without illumination and (b) with illumination.	102
Figure 4. 16: (a) Transfer characteristics, and (b) output characteristics of TFT fabricated on 135 nm ZnGa ₂ O ₄ epilayer. (c) D-mode, and (d) E-mode of operation of the transistor.	103
Figure 4. 17: (a) Responsivity as a function of wavelength, and (b) time response of the Neutral ion beam etched PT.	105
Figure 5. 1: Fabrication process flow of the Transmission line measurement contacts on the ZnGa ₂ O ₄ film.	113
Figure 5. 2: Schematic of TLM contacts with the distance between contact as 10, 20, 30, 40, 50, and 60 μm.	113
Figure 5. 3: (a) Energy of gold ions versus the nuclear energy loss (S _n) and electronic energy loss (S _e) (b) cross-sectional FESEM of the ZnGa ₂ O ₄	115
Figure 5. 4: X-ray 2 theta scan patterns of the ZnGa ₂ O ₄ thin film (a) over a broad range from 15° to 70°, and (b) 111, (c) 222, and (333) peak, before and after irradiation.	116
Figure 5. 5: Williamson Hall analysis of the bare and irradiated ZnGa ₂ O ₄ film.	117
Figure 5. 6: AFM images of the ZnGa ₂ O ₄ thin film (a) before and after irradiation of gold ions at fluences (b) 1 × 10 ¹² ions/cm ² , (c) 5 × 10 ¹² ions/cm ² , (d) 7 × 10 ¹² ions/cm ² , and (e) 1 × 10 ¹³ ions/cm ²	118
Figure 5. 7: (a) Survey spectra, (b) Ga 2p, and (c) Zn 2p XPS spectra of the ZnGa ₂ O ₄ thin film before and after irradiation at ion fluences of 1 × 10 ¹² , 5 × 10 ¹² , 7 × 10 ¹² , and 1 × 10 ¹³ ions/cm ²	119
Figure 5. 8: XPS O 1s spectra of the ZnGa ₂ O ₄ thin film (a) before and after gold irradiation at fluences (b) 1 × 10 ¹² ions/cm ² , (c) 5 × 10 ¹² ions/cm ² , (d) 7 × 10 ¹² ions/cm ² , and (e) 1 × 10 ¹³ ions/cm ² . (f) Relative percentages of oxygen vacancies as a function of ion fluence.	119
Figure 5. 9: (a) UV-visible absorbance spectra and (b) Tauc plot for the bare and irradiated ZnGa ₂ O ₄ thin film.	122
Figure 5. 10: Water contact angle measurements for ZnGa ₂ O ₄ thin film before and after gold irradiation.	123

Figure 5. 11: EPMA of the transmission line measurement contacts fabricated on the ZnGa ₂ O ₄ film for electrical characterization.	125
Figure 5. 12: I-V curves of the ZnGa ₂ O ₄ thin film (a) before, and after gold irradiation at a contact distance of 10 μm. Transmission line measurements of (b) bare, and gold irradiated film with fluence (c) 1 × 10 ¹² ions/cm ² , (d) 5 × 10 ¹² ions/cm ² , (e) 7 × 10 ¹² ions/cm ² , and (f) 1 × 10 ¹³ ions/cm ²	125
Figure 5. 13: Resistance versus the distance between contact plots for (a) bare and irradiated film at fluence of (b) 1×10 ¹² , (c) 5×10 ¹² , (d) 7×10 ¹² , and (e) 1×10 ¹³ ions/cm ²	127
Figure 5. 14: Radar chart comparing the obtained differences in the bare and the gold ion irradiated film at a fluence of 10 ¹³ ions/cm ²	128
Figure 6. 1: Schematic for the preparation of copper oxide nanowires.....	135
Figure 6. 2: X-ray diffraction pattern of the (a) Copper foil and (b) thermally oxidized copper foil in argon, oxygen, and air.	137
Figure 6. 3: FESEM images of samples grown in (a) argon, (b) air, (c) oxygen, and (d) cross-sectional view of the synthesized sample in oxygen, respectively.	138
Figure 6. 4: SEM images of the CuO nanowire and the diameter of the labeled nanowires.	138
Figure 6. 5: HRTEM images of the (a) nanowire, (b) fringes of the nanowire, and (c) SAED pattern of the nanowire grown in an oxygen environment...	140
Figure 6. 6: (a) Raman and (b) UV-visible spectrum of the as-synthesized samples.	141
Figure 6. 7: a) Survey spectrum, and (b) Copper 2p spectrum for the as-synthesized samples.	143
Figure 6. 8: Deconvoluted spectra of Cu 2p _{3/2} for samples grown in (a) air, (b) argon, and (c) oxygen environment. (d) The relative concentration of Cu ²⁺ to Cu ⁺ on the surface of the as-synthesized samples.	144
Figure 6. 9: XPS O 1s Spectrum for samples prepared in a) oxygen, b) argon, and c) air.	145
Figure 6. 10: Contact angle measurements of bare copper and samples prepared in air, oxygen, and argon.	147

Figure 6. 11: (a) Schematic of the PEC splitting, and (b) photocurrent density for samples synthesized in air, oxygen, and argon. The photocurrent density (c) time response, and (d) stability for the sample synthesized in an oxygen environment..... 151

Figure 6. 12: Mott Schottky plots of samples prepared in (a) argon, (b) air, and (c) oxygen. (d) Electrochemical impedance spectra of the grown samples. 153

LIST OF TABLES

Table 1. 1: Material properties of ZnGa ₂ O ₄	11
Table 1. 2: Performance parameters of the photodetectors.	19
Table 3. 1: Rise and fall times of the ZnGa ₂ O ₄ and β-Ga ₂ O ₃ DXPDs exposed to hard X-rays at different irradiation-dose levels.....	61
Table 3. 2: Binding Energy of the electrons for elements in their natural form.	63
Table 3. 3: Sensitivity of ZnGa ₂ O ₄ and β-Ga ₂ O ₃ hard DXPDs.	66
Table 3. 4: Performance comparison with other detectors.	68
Table 4. 1: Performance parameters comparison with the reported MOSFETs:	96
Table 4. 2: Threshold voltage of ZnGa ₂ O ₄ PT operated at different drain voltage with 240 nm and in dark conditions.....	99
Table 4. 3: Performance benchmarks.....	106
Table 5. 1: SRIM calculations of the 120 MeV gold ions in the ZnGa ₂ O ₄ film.....	115
Table 5. 2: X-ray 2-θ scan peak positions, crystallite size, and lattice strain of the ZnGa ₂ O ₄ thin film before and after irradiation.....	116
Table 5. 3: Peak positions and subsequent percentage concentration of oxygen vacancy in the bare and irradiated films.....	120
Table 6. 1: Peak positions and subsequent percentage concentration of copper in as-synthesized samples.....	144
Table 6. 2: Comparison with the previously fabricated copper oxide-based electrodes.	149

ABBREVIATIONS

MOCVD	Metal organic chemical vapor deposition
DXPD	Metal semiconductor metal
MSM	Direct irradiating X-ray photodetector
TFT	Thin film transistor
PT	Phototransistor
SRIM	The stopping and range of ions in matter
PEC	Photoelectrochemical
SBH	Schottky barrier height
I-V	Current Voltage
ZGO	Zinc gallium oxide
CVD	Chemical vapor deposition
CA	Contact angle
TLM	Transmission line measurements
XRD	X-ray diffraction
UV	Ultraviolet
FESEM	Field electron scanning electron microscopy
XPS	X-ray photoelectron spectroscopy
B.E.	Binding energy
MFC	Mass flow controller
DFT	Density functional theory
EPMA	Electron probe microanalyzer
TEM	Transmission electron microscopy
HRTEM	High-resolution transmission electron microscopy
AFM	Atomic force microscopy
ICP	Inductively coupled plasma
JCPDS	Joint Committee on Powder Diffraction Standards
BSE	Backscattered electron
ALD	Atomic layer deposition
IGPS	Integrated gas phase synthesis setup
PVD	Physical vapor deposition

CB	Conduction band
VB	Valance band
KPFM	Kelvin probe force microscopy
SHI	Swift Heavy Ion